LOW-FIELD NEUROIMAGING: THEORY VS. DATA

Validation of High-Performance Low-Field-Strength T1-weighted neuroimaging sequence modelling

T. Whyntie[1], K.-Y. Chu[1], V. Dhanda[2], D. Hughes[2], T. Patel[2], S. Teoh[1], T. Maughan[1]

[1]MRC Oxford Institute for Radiation Oncology, University of Oxford, UK
[2]GenesisCare, Oxford, UK

OHBM 2021 virtual poster number: 1123
Corresponding author: Tom Whyntie. *Email*: tom.whyntie@oncology.ox.ac.uk

Introduction

High-Performance Low-Field-Strength (HPLFS) MRI, i.e. <1T magnets driven by modern hardware and software systems, may make MRI more widely available and offer new clinical opportunities (Campbell-Washburn, 2019). Here we explore low-field neuroimaging (Marques, 2019) with a simple model of a gradient echo sequence and compare predicted and measured performance at 0.35T and 3T using images of the same healthy volunteer, acquired as part of technical development studies in line with our institution's ethics guidelines.

0.35T Image Acquisition

Low-field images were acquired on the imaging system of a clinical MR-Linac (MRIdian® system; ViewRay Inc., Cleveland, OH, USA) using two five-element phased-array head and neck coils and a T1-weighted RF-spoiled gradient echo sequence with parameters TR/TE = 20/6.23ms and a flip angle of 30 degrees.

3T Image Acquisition

High-field images were acquired on a research 3T Siemens MAGNETOM Prisma (Siemens Healthcare, Erlangen, Germany) using a 32-channel phased-array head coil and the UK Biobank standard T1-weighted MP-RAGE sequence (Alfaro-Almago, 2018) with parameters TR/TE/TI: 2000/2.03/880ms and a flip angle of 8 degrees.

Theory

Reducing the field strength alters the tissue relaxation times and reduces the overall MR signal, increasing the impact of noise on the SNR and CNR.

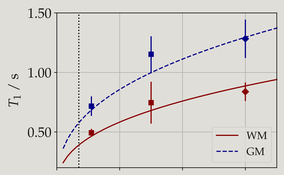

Relaxation times

T_1 estimation - see (Bottomley, 1984).

Experimentally-determined values

Longitudinal relaxation time — $T_1 = A_1 \left[\gamma_p B_0\right]^{b_1}$

Proton gyromagnetic ratio — *Field strength*

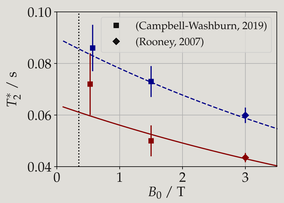

T_2 estimation - see (Pohmann, 2016).

Experimentally-determined values

Apparent transverse relaxation time — $T_2^* = A_2 e^{-b_2 B_0}$

Field strength

White Matter (WM): T_1 / T_2 = 390/61ms
Grey Matter (GM): T_1 / T_2 = 578/86ms

The gradient echo signal

Proton density — *Echo time*

$$S_{SGE} \propto \rho \frac{(1-E_1)\sin\alpha}{1-E_1\cos\alpha} e^{-\frac{TE}{T_2}}$$

(Fram, 1987) — *Flip angle*

$$E_1 = e^{-\frac{TR}{T_1}}$$

Repetition time

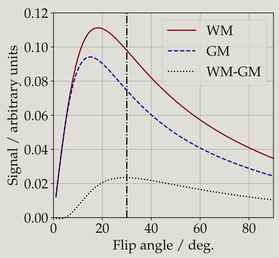

For TR/TE = 20/6.23ms as in the plot, the optimal flip angle is 30 degrees.

Noise estimation

We can estimate the ratio of the high- (H) and low-field (L) noise as follows:

Acquisition efficiency

Noise, as per Eq. 9 (Reeder, 1994) —

$$\frac{\sigma_H}{\sigma_L} = \frac{\Delta V_H}{\Delta V_L}\sqrt{\frac{\eta_H}{\eta_L}}\sqrt{\frac{t_H}{t_L}}$$

Voxel volume — *Acquisition time*

Thus the low-field noise can be estimated from the high-field noise data.

Acq. time: 351s (5 min. 51s)
No. slices x matrix: 144 x 180 x 188
Acq. speed: 13,883 voxels/s
Voxel size: 1.5mm (isotropic)
WM SNR: 12.9 (9.4 pred.)
GM SNR: 8.0 (6.9 pred.)
WM-GM CNR 1.7 (1.3 pred.)
ICV: 1.562dm^3

Acq. speed: 46,052 voxels/s
No. slices x matrix: 208 x 256 x 256
Acq. time: 296s (4 min. 56s)
WM SNR: 21.3
Voxel size: 1.0mm (isotropic)
GM SNR: 13.7
WM-GM CNR 4.9
ICV: 1.563dm^3

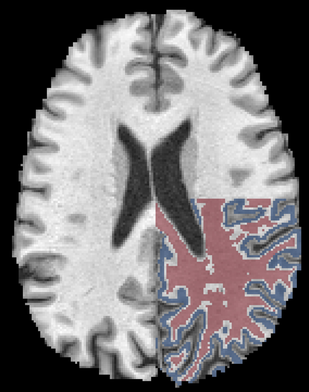

The 3T pure WM/GM masks from FAST were transformed to the 0.35T image space. Note that these slices are not registered, so appear slightly different.

Image Processing, Harmonisation, and Analysis Methods

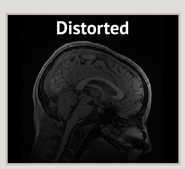

Gradient distortions are corrected either on-scanner (0.35T) or with gradunwarp (3T) (Jovicich, 2006).

Brain extraction is performed with FSLanat, as per the UK Biobank processing pipeline (Alfaro-Almagro, 2018), (Jenkinson, 2012). Mask volume provides the Intracranial Volume (ICV) measurement.

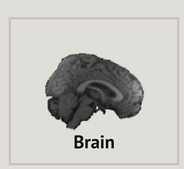

FSLanat also runs FAST (Zhang, 2001) for bias field correction and tissue segmentation. Intensities are harmonised by aligning pure WM peaks. Registration perfomed with FLS's FLIRT.

Results

Representative axial slices, along with key results, are shown in the panels to the left. For the high-field images, the mean and s.d. of the pure tissue intensities are used for SNR and CNR calculations (Alfaro-Almagro, 2018).

FAST assumes pure tissue intensity is normally distributed when segmenting the brain. The peaks can be seen in the brain intensity PDF at 3T.

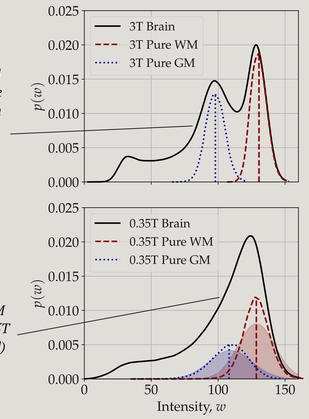

Data from the 3T FAST pure tissue voxels were used for SNR and CNR calculations, as per (Alfaro-Almagro, 2018).

The distinct WM/GM peaks are lost at 0.35T due to the (predicted) loss in contrast.

The measured GM signal is 85% of the WM signal, which compares well with the predicted 84%.

The measured WM/GM noise values (dashed/dotted lines) are slightly better than predicted (shaded regions).

The low-field brain was registered to the high-field image (FSL's FLIRT, 6 d.o.f.), and the transformation was then applied to the 3T pure tissue masks. These masks were used to extract the 0.35T pure tissue properties.

Conclusions

For similar scan times (~5 min.), the SNR and CNR for WM and GM were predicted to reduce by roughly half and a third respectively with a field strength of 0.35T. While the 0.35T data slightly improved on these predictions, a reduction in performance was confirmed. Although the particular low-field sequence used here may not be suitable for e.g. quantitative structural analysis, the techniques presented could be used in the evaluation of more efficient sequences, such as the non-Cartesian schemes proposed in (Campbell-Washburn, 2019). Such improvements could pave the way for deploying HPLFS MRI systems in harder-to-reach locations (e.g. critical care wards for strokes), portable permanent magnet-based systems, or MR-guided Proton Therapy systems where lower magnetic field strengths are desirable.

"We have measured and quantified low-field neuroimaging performance with respect to standard high-field clinical sequences using data-driven harmonisation techniques."

References

Alfaro-Almagro, F. et al. (2018), NeuroImage, vol. 166, pp. 400-424 doi:10.1016/j.neuroimage.2017.10.034
Bottomley, P.A. et al. (1984), Medical Physics, vol. 11, no. 4, pp. 425-448 doi:10.1118/1.595535
Campbell-Washburn, A.E. et al. (2019), Radiology, vol. 293, no. 2, pp. 384-393 doi:10.1148/radiol.2019190452
Fram, E. K. et al. (1987), Magnetic Resonance Imaging, vol. 5, no. 3, pp. 201-208 doi: 10.1016/0730-725X(87)90021-X
Jenkinson, M. et al. (2012), NeuroImage, vol. 62, no. 2, 782-790 doi:10.1016/j.neuroimage.2011.09.015
Jovicich, J. et al. (2006), NeuroImage, vol. 30, pp.436-443 doi:10.1016/j.neuroimage.2005.09.046
Klüter, S. (2019), Clinical and Translational Radiation Oncology, vol. 18, pp. 98-101 doi: 10.1016/j.ctro.2019.04.007
Marques, J.P. et al. (2019), Journal of Magnetic Resonance Imaging, vol. 49, no. 6, pp. 1528-1542 doi:10.1002/jmri.26637
Pohmann, R. et al. (2016), Magnetic Resonance in Medicine, vol.75, no. 2, pp. 801-809 doi:10.1002/mrm.25677
Reeder, S.B. et al. (1994), Magnetic Resonance in Medicine, vol. 32, no. 5, pp. 612-621 doi:10.1002/mrm.1910320510
Rooney, W.D. et al. (2007), Magnetic Resonance in Medicine. vol. 57, no. 2, pp. 308-318 doi:10.1002/mrm.21122
Sudlow, C. et al. (2015) PLoS Medicine, Vol. 12, no.13, pp. 1-10 doi:10.1371/journal.pmed.1001779
Zhang, Y. et al. (2001), IEEE Transactions on Medical Imaging, vol. 20, no. 1, pp.45-57 doi:10.1109/42.906424

The authors would like to acknowledge M. Jenkinson, E. Duff, J. Campbell and the FSL Development Team at the Wellcome Centre for Integrative Neuroimaging (WIN), University of Oxford, for support with the high-field image acquisition, harmonisation, and analysis. Parts of this work was funded by the NIHR Biomedical Research Centre, Oxford; Cancer Research UK; and carried out as part of the University's Research Collaboration with GenesisCare UK. The views expressed are those of the authors and not necessarily those of the NHS, the NIHR, the Department of Health, or GenesisCare UK. The authors declare no Conflicts of Interest.